sciendo

DOI 10.2478/ama-2023-0062

acta mechanica et automatica, vol.17 no.4 (2023)
Special Issue "Modeling of materials with nano/microstructure"

THE STUDY OF TEMPERATURE-DEPENDENT MAGNETIC PROPERTIES VARIATION IN CoCr2O4 NANOPARTICLES WITH (y = 0.8) AND WITHOUT COATING CONCENTRATION OF NON-MAGNETIC (SiO2)y

Ghazanfar MEHBOOB*, Kashif NADEEM, Amjad IQBAL*****
Gohar MEHBOOB****, Shahnawaz HUSSAIN*, Mohamed RAGAB*******
Mazhar IQBAL******, Sohaib AJMAL*********, Adel EL-MARGHANY**********

*State Key Laboratory for Mechanical Behavior of Materials, School of Materials Science and Engineering, Xi'an Jiaotong University, Xi'an, 710049, China
**Department of Physics, International Islamic University Islamabad, Pakistan
***Faculty of Materials Engineering, Sileisan University of Technology, Gliwice 44-100, poland
****School of Materials Science and Engineering, South China University of Technology, Guangzhou, China
*****Department of Mechanical Engineering (Production and Design), Shoubra Faculty of Engineering, Benha University, Benha 13512, Egypt
******Department of Physics, University Azad Jammu and Kashmir, Muzaffarabad, Pakistan
*******Institute for Advanced Ceramics, School of Materials Science and Engineering, Harbin Institute of Technology, Harbin, 150080 China
********Department of Chemistry, College of Science, King Saud University, P.O. Box 2455, Riyadh 11451, Saudi Arabia

ghazanfar3152@stu.xjtu.edu.cn, kashif.nadeem@iiui.edu.pk, amjad.iqbal@polsl.pl
goharmehboob125@hotmail.com, shahnwazhussain904@hotmail.com, mohamed.emam01@feng.bu.edu.en
mazhariqbal5252@gmail.com, sohaibajmal905@hit.edu.cn, amarghany@ksu.edu.sa

received 31 January 2023, revised 12 April 2023, accepted 04 June 2023

Abstract: The present study investigates the temperature-dependent magnetic (MT) properties of CoCr2O4/(SiO2)y (y = 0 and 0.8) nanoparticles. Nanoparticles were synthesised by using the conventional sol–gel technique. The X-ray diffraction (XRD) method confirmed the normal spinel structure of CoCr2O4 nanoparticles. The main peak analysis of the XRD pattern using Debye–Scherrer's formula probes the mean crystallite sizes for coated and uncoated nanoparticles, and the sizes based on which the probes have been carried out amount to 19 nm and 28 nm, respectively. The transmission electron microscopy (TEM) image showed the non-spherical shape of these nanoparticles. Field-cooled (FC) and zero field-cooled (ZFC) MT plots were taken by using a superconducting quantum interference device (SQUID) magnetometer. Pure CoCr2O4 nanoparticles showed the ferrimagnetic transition at Curie temperature (Tc = 99 K) on an applied field (H) of 50 Oe. Tc decreased up to 95 K with the increase in 80% SiO2 concentration in CoCr2O4 nanoparticles. For pure samples, conical spiral temperature (TS) and lock-in transition temperature (TL) remain unchanged with increasing magnetic field because of strong spin–lattice coupling. However, for 80% SiO2 impurity, the decrease in Tc was attributed to the reduction in surface disorder with a minor decline in TS and TL. The Ms declined with a decrease in temperature because of the existence of stiffed/strong conical spin-spiral and lock-in states in pure CoCr2O4 nanoparticles, while nanoparticles with 80% coating SiO2 concentration showed abnormal behavior. The coercivity increases with a decrease in temperature due to a decrease in thermal fluctuations at low temperatures for both samples. The fitting of coercivity (Hc) versus temperature plot by using Kneller's law has given the values of coercivity constant (α) and coercivity at average blocking temperature (TB) for both samples, which are α = 0.54, TB = 75 K and α = 1.59, TB = 81 K, respectively. Hence, the increase in the concentration of SiO2 decreased nanoparticles size and surface disorder in CoCr2O4 nanoparticles while enhancing Ms below spin-spiral state ordering.

Key words: cobalt chromite, sol-gel synthesis, nanoparticles, corrosion, magnetic properties

1. INTRODUCTION

Ferri/ferromagnetism and ferroelectric coupling in heterostructure material or single material are used in many electronic devices as sensors and data storage devices and are chemically used as ferro-fluids, radar-absorbing paint, drug delivery, power transformer cores, the oxidation of 2-propanol [1] industrial inorganic pigment [2], solar absorber [3], electrode in solid oxide fuel cell (SOFCs) [4,5], catalyst support [6], etc. Most of the research activities have been precipitated due to the scientific engrossment in multiferroicity [7]. Scientists have an attraction towards nanometre range spinel metal oxides because of their broad range of functions in solid-state sciences [8]. Chromites with the general formula ACr2O4 have a normal spinel structure, where A indicates the divalent metallic ions (Ni2+, Zn2+, Mn2+, Cu2+, Fe2+, Co2+, Mg2+, etc.) at the tetrahedral (T) site and trivalent chromite ion (Cr3+) lies at the octahedral site [9, 10]. A majority of the applications of spinel magnetic nanoparticles as multiferroic material are due to their intrinsic properties such as low dielectric losses, low coercivity (Hc), high resistivity, high chemical stability and high saturation magnetisation (Ms) [11]. Cobalt chromite (CoCr2O4) has greenish-blue pigments, which are crystallised in cubic Fd3m structure having lattice constant a = 8.33 Å with Co2+ ions at the tetrahedral site and Cr3+ ions at the

octahedral site [12]. Bulk CoCr2O4 has paramagnetic (PM) to ferromagnetic (FM) magnetic phase transition temperature (Tc), conical spiral temperature (TS) and lock-in transition temperature (TL) of 94 K, 27 K and 15 K, respectively [13]. According to Menyuk et al. [14], the cobalt chromite magnetic order incorporates a spin-spiral FM state below Tc. The spiral component exhibits short-range order at a temperature of 86 K, which then transmutes into long-range order at a temperature of 31 K, while the FiM component for all temperatures below Tc exhibits long-range order. The spiral long-range order of FiM was estimated by cone angle 'u' [15] as

$$u = 4SBJBB/3SAJAB. \quad (1)$$

Here, *SA* and *SB* are the magnitudes of spin at A site and B site, respectively; similarly, *J*AB and *J*BB are the nearest exchange interactional spins between A–B sites and B–B sites, respectively. It was experimentally found that the value of cone angle for FM long-range spiral order is u = 2. In the case of bulk CoCr2O4, *J*BB interactions are strong between two chromium ions and have a significant role in cone angles of the long-range spiral state (*TS*) [16]. The cobalt chromite (CoCr2O4) nanomaterial has no magnetic response in the low-temperature range. The magnetic phase transition is gigantic and uncommon in CoCr2O4 with *TL* = 8 K, *TS* = 31 K and *Tc* = 100 K [17]. It was observed that *TS* remained the same for bulk along with nano CoCr2O4 due to strong interaction between B–B sites. The long-range spiral states stipulate the supremacy of B–B interactions on A–B interactions.

The spins at the surface of the nanoparticles efficiently control magnetic properties for surface action and other applications [18]. CoCr2O4 nanoparticles have a high tendency to agglomerate due to their magnetic nature [19]. Agglomeration can be reduced by coating nanoparticles with non-magnetic material. Usually, Al2O3, SiO2 and TiO2 are used for this purpose [20]. SiO2 is the most efficient and commonly used non-magnetic material for the coating of nanoparticles [21], as it controls the interparticle interactions through its shell thickness, and controls also the surface effects and the size of particles; additionally, it is also characterised by excellent stability [22]. A large number of nucleation sites are formed smaller in size and single phase during the synthesis process when nanoparticles are coated with SiO2 as SiO2 reduces the growth of nanoparticles [23–25]. Consequently, the magnetic properties of multiferroic nanomaterials can be controlled by SiO2 coating, which will also affect the magneto-electric coupling [26].

Therefore, the SiO2 non-magnetic material coating has a great effect on the CoCr2O4 nanoparticle's magnetic properties, which is required to be studied for its useful applications in modern technology. In this study, we have probed the magnetic response on both coated and uncoated CoCr2O4 nanoparticles with SiO2 at different temperature ranges.

2. RESULTS AND DISCUSSION:

Figure 1 displays the X-ray diffraction (XRD) plots for CoCr2O4/(SiO2)y nanoparticles produced by the sol–gel method at y = 0% and 80%. Indexed peaks (111), (220), (311), (400), (422), (511) and (440) of XRD plots revealed the cubic structure of both coated and uncoated CoCr2O4 nanoparticles (JCPDS file No.: 780711).

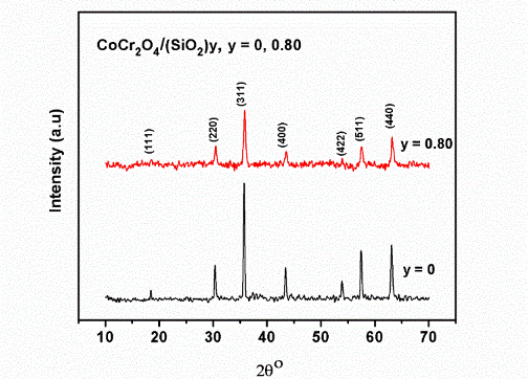

Fig. 1. The XRD patterns of CoCr2O4/(SiO2)y (y = 0% and 80%) nanoparticles. XRD, X-ray diffraction

For both cases, the positions of peaks almost remain the same, which indicated that the coating of SiO2 did not alter the internal structure of CoCr2O4 nanoparticles. The intensities of all the peaks have been reduced for coated nanoparticles. No peaks of silica were found in the XRD scan because its nature is amorphous.

The sizes of nanoparticles (D) were probed by the main peak (311) investigation of XRD patterns by using Debye–Scherrer's equation:

$$D = \frac{0.9\lambda}{\beta cos\theta}, \quad (2)$$

where λ is the wavelength of the X-ray, β is the full width at half maximum (FWHM) of the plane hkl and $\boldsymbol{\theta}$ is the Bragg angle.

The mean crystallite sizes of CoCr2O4/(SiO2)y (y = 0 or 0.80) nanoparticles with y = 0 and y = 0.80 are 28 nm and 19 nm, respectively. The mean crystallite size of nanoparticles is decreased with an increase in the concentration of silica because of the increase in the number of nucleation sites in the SiO2 matrix under the process of synthesis, which stops the further growth of nanoparticles [24, 25, 27, 28].

Transmission electron microscopy (TEM) was used to observe the nanoparticles' shape, size and agglomeration. Figure 2 reveals the TEM image, at 100 nm scale, of cobalt chromite (CoCr2O4/(SiO2)y) nanoparticles with y = 0. From Fig. 2, we observe the elongated/irregular shape of nanoparticles. However, a certain degree of agglomeration is also exhibited because of the magnetic interactions among nanoparticles [29, 30].

The superconducting quantum interference device magnetometer (SQUID Quantum Design, MPMS-XL-7) was used to measure the magnetic properties of CoCr2O4/(SiO2)y (y = 0 or 0.80) nanoparticles.

Figures 3(a,b) reveal the T-dependent zero field-cooled (ZFC) and field-cooled (FC) magnetisation curves of CoCr2O4/(SiO2)y (y = 0 or 0.80) nanoparticles at different applied magnetic fields of 50 Oe, 500 Oe and 1,000 Oe. The sample was cooled from 145 K to 4.2 K and then magnetisations were recorded with FC and without ZFC applied magnetic field in increasing temperature from 4.2 K to 145 K. FC measurements were taken for different applied magnetic fields of values 50 Oe, 500 Oe and 1,000 Oe [31]. Negative magnetisation was observed in ZFC curves for both

sciendo
DOI 10.2478/ama-2023-0062

samples with y = 0 and y = 0.8 in the temperature ranges of 4.2–87 K and 4.2–71 K, respectively, owing to uncompensated spins at the grain boundaries. The negative magnetisation decreases with increasing the external magnetic field in both cases as more and more magnetic moments are aligned along the magnetic field direction concomitant with an increase in the external magnetic field. From graphs of CoCr2O4/(SiO2)y (y = 0 and 0.80) nanoparticles, the obtained results show that the negative magnetisation decreased with the silica coating of CoCr2O4 nanoparticles. It means that SiO2 coating results in a decrease in the orderings of surface spins of nanoparticles [13, 32, 33]. The temperature at which the material changes its state from paramagnetic to ferrimagnetic in both ZFC and FC conditions is called Curie temperature (*TC*), while the dip associated with *Ts* is responsible for the conical spiral state. ZFC/FC plots for a sample with y = 0 taken at 50 Oe, 500 Oe and 1,000 Oe have conical spinal state *TS* = 27 K and *TC* at 99 K, 100 K and 101 K, respectively, which were confirmed by the values already reported by Plocek et al. [34] and Plumier et al. [35]. ZFC/FC plots for the sample with y = 0.80 at 50 Oe, 500 Oe and 1,000 Oe have conical spinal state *TS* at 19 K, 25 K and 25 K, respectively, and similarly *TC* at 95 K, 99 K and 100 K, respectively.

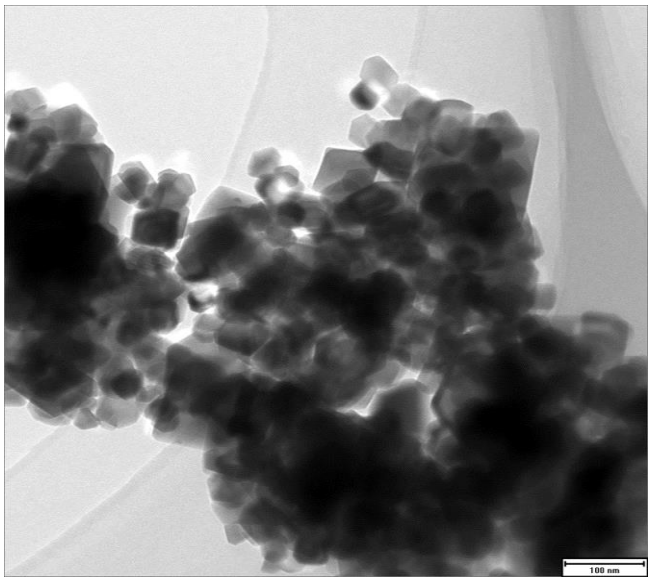

Fig. 2. TEM image of cobalt chromite without silica concentration nanoparticles at 100 nm scale. TEM, transmission electron microscopy

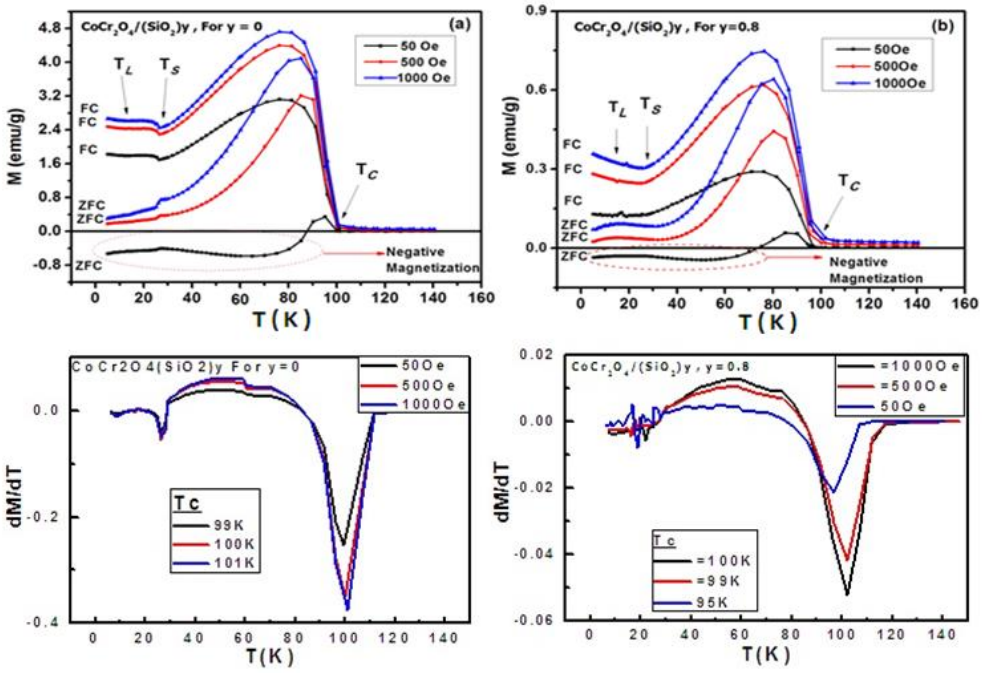

Fig. 3. ZFC/FC curves for cobalt chromite nanoparticles with (a) 0% silica concentration and (b) 80% silica concentration at different applied fields. FC, field cooled; ZFC, zero field cooled

Low-temperature lock-in state (at which spiral spins lock to lattice parameter) occurs at TL = 12 K for the sample with y = 0 and occurs at TL = 11.5 K, TL = 15 K and TL = 17 K under applied fields of 50 Oe, 500 Oe and 1,000 Oe, respectively, for the sample with y = 0.8. TL and TS did not exhibit any dependence on the external field due to strong spin–lattice coupling at low temperatures [36] for the sample with y = 0. TL, TS and TC are decreased for the sample with y = 0.80 due to the decrease in their crystallite size as compared to the sample with y = 0 [37, 38]. The values of TL, TS and TC for CoCr2O4/(SiO2)y (y = 0 and y = 0.80) nanoparticles at the various external fields of 50 Oe, 500 Oe and 1,000 Oe are mentioned in Table 1.

In order to study the coercivity (*HC*) and saturation magnetisation (*MS*) of cobalt chromite nanoparticles owing to surface and magnetic transitional effects, the T-dependent M–H loops have been taken into consideration. Figure 4 depicts M–H loops of cobalt chromite (CoCr2O4) nanoparticles with 0% concentration of silica under ±5 T field at the different constant temperatures of 5 K, 25 K, 50 K and 75 K. The inset of Figure 4 displays the expanded region for *HC*. All loops show a ferrimagnetic trend that contains the ZFC/FC results. The M–H loops of nanoparticles are not fully saturated at field ±5 T because

of their random surface spins, which necessitated a rather high field for complete saturation.

Tab. 1. The TL, TS and TC values for chromite nanoparticles (CoCr2O4) with 0% and 80% silica concentrations at different external fields

Concentration	Field	T_C	T_S	T_L
0%	50 Oe	99 K	27 K	12 K
	500 Oe	100 K	27 K	12 K
	1,000 Oe	101 K	27 K	12 K
80%	50 Oe	95 K	19 K	11.5 K
	500 Oe	99 K	25 K	15 K
	1,000 Oe	100 K	25 K	17 K

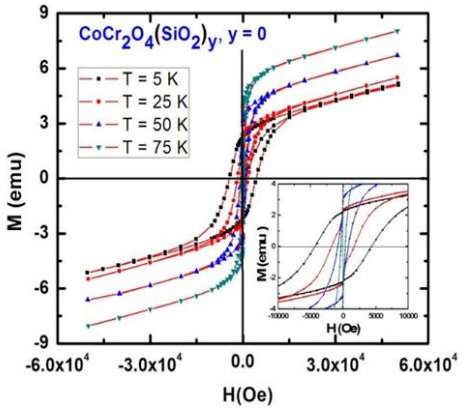

Fig. 4. M–H loops of cobalt chromite nanoparticles with 0% concentration of silica at the different constant temperatures of 5 K, 25 K, 50 K and 75 K

The values of *MS* and *HC* are presented in Figure 4. The value of *MS* is calculated at constant temperature $T = 5$ K, which is 5.1 emu/g. Figure 5(a) shows variation in *Ms* with respect to different temperatures for CoCr2O4 nanoparticles with 0% silica concentration. The *Ms* graph has shown decreasing trend with decreasing temperature, which does not show an accordance with the prediction of Bloch's law for ferro-ferrimagnetic materials. This trend is attributable to the presence of stiffed/strong conical spin-spiral and lock-in states at low temperatures. From M–H loops, we have also found the value of *HC*. Figure 5(b) reveals the value of *HC* at different temperatures. *HC* reveals a decreasing trend with increasing temperature by a decrease in thermal fluctuations [39–41]. At high temperatures, the spin-flip time is less than the measurement time because thermal energy is greater than anisotropic energy; therefore, the particle reveals a lower value of *HC*. By decreasing the temperature, the thermal energy will be decreased, and the thermal energy is less than anisotropic energy at low temperatures and shows a higher *HC* value.

Figure 6 exhibits the M–H loops of cobalt chromite (CoCr2O4) nanoparticles with an 80% concentration of silica at the different temperatures of 5 K, 15 K, 25 K, 50 K and 75 K. The value of *MS* is 2.16 emu/g at a temperature of 5 K. Since the crystallite size of nanoparticles without silica concentration is greater than that of nanoparticles with silica concentration, as far as the nanoparticles with a 0% silica concentration are concerned, their *Ms* value is higher in comparison with nanoparticles with an 80% silica concentration. This means that the *MS* value depends mainly upon the crystal size. The smaller the size of the crystal, the lower will be the value of *Ms*. The reduction in *MS* value is also owing to the fact of increase in the surface-to-volume ratio [42]. The M–H loops of cobalt chromite (CoCr2O4) nanoparticles with silica concentrations at various temperatures are less saturated even at a high field (5 T) if compared to the nanoparticles without silica concentration due to surface effects.

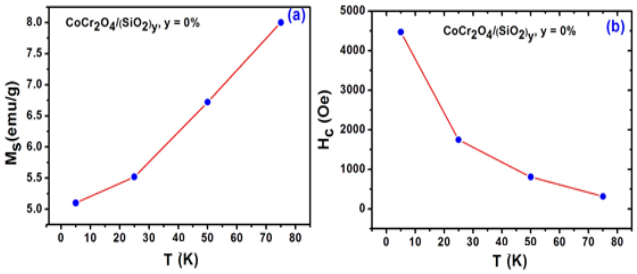

Fig. 5. The variation in (a) saturation magnetisation and (b) coercivity with the temperature of CoCr2O4 nanoparticles with 0% concentration of silica

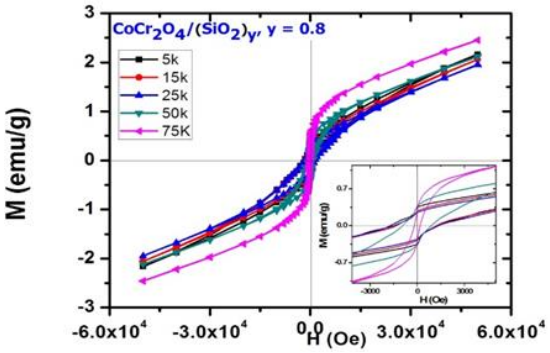

Fig. 6. M–H loops of cobalt chromite nanoparticles with 80% concentration of silica at the different temperatures of 5 K, 15 K, 25 K, 50 K and 75 K

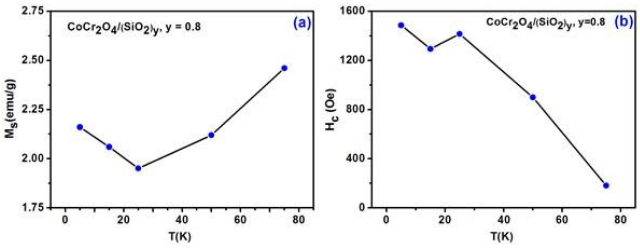

Fig. 7. The variation in (a) saturation magnetisation and (b) coercivity with temperature of CoCr2O4 nanoparticles with 80% concentration of silica (solid lines just show the trend)

Figure 7a shows the trend of the *Ms* value of nanoparticles with silica concentration at different constant temperatures. From M–H loops of CoCr2O4 nanoparticles with silica concentration, the *MS* values reveal abnormal behaviour attendant with changes in temperature due to non-magnetic silica coating. The SiO2 coating can enhance surface disorder by creating a surrounding layer around the nanoparticles [43]. There is an increase in *Ms* value below 25 K, which is attributed to a change in the spin-spiral state due to SiO2 coating. Figure 7b reveals the trend of temperature-dependent *Hc* for CoCr2O4 nanoparticles with an 80% concentration of silica. The value of *Hc* also shows a decreasing trend with increasing temperature. *Hc* of nanoparticles

depends upon many factors such as core anisotropy, coating material, annealing temperature, size of the particle, dipole interaction and surface anisotropy [44].

Figure 8 reveals the combined behaviour of saturation magnetisation and coercivity with the temperature of CoCr2O4 nanoparticles for both 0% and 80% concentrations of silica. The saturation magnetisation behaviour with temperature for nanoparticles with silica concentration is different from nanoparticles without silica concentration, as observed in Figure 8a. The saturation magnetisation for nanoparticles with no silica concentration has decreased with decreasing temperature, while for nanoparticles with silica concentration, its value has increased with decreasing the temperature at a temperature below 25 K. Therefore, this region is called the conical spin-spiral region, in which both magnetic dipoles and electric dipoles are existing at the same phase. The behaviour of coercivity with temperature for CoCr2O4 nanoparticles without silica concentration was changed with the concentration of silica, as shown in Figure 8b. The sharp increment in coercivity in nanoparticles without silica concentration is not observed in nanoparticles with silica concentration, which means that surface anisotropy has reduced in nanoparticles with the concentration of silica.

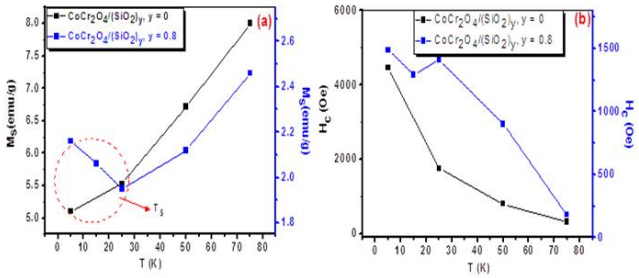

Fig. 8. (a) Saturation magnetisation with temperature and (b) coercivity with temperature of CoCr2O4 nanoparticles with and without silica concentration (solid lines just show the trend)

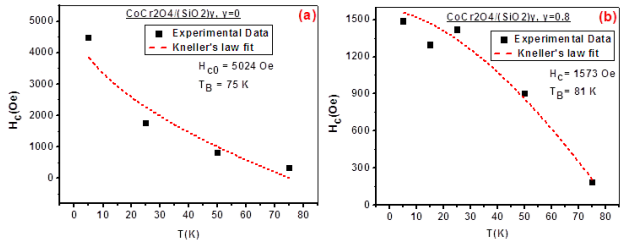

Fig. 9. Kneller's law fit for CoCr2O4 nanoparticles (a) without and (b) with silica concentration

The experimental data of coercivity of CoCr2O4 nanoparticles without and with silica concentration are fitted using Kneller's law. The *HC* for randomly oriented non-interacting nanoparticles (uniaxial anisotropy and single domain) can be clarified using Kneller's law [45] as follows:

$$Hc = Hc0\,[1 - (T/TB)\alpha], \tag{3}$$

where *HC*, *HC*0 and *TB* are the coercivities at any temperature, at a temperature of 0 K and at average blocking temperature, respectively. Figure 9 reveals Kneller's law fitting for CoCr2O4 nanoparticles with and without silica concentration. The best of Kneller's law fit for nanoparticles with no silica concentration reveals fitting parameters as $\alpha = 1.54$ and $TB = 75$ K, and for nanoparticles with silica concentration as $\alpha = 1.59$ and $TB = 81$ K. Kneller's law diverges at lower temperatures for nanoparticles with no silica concentration due to strong interparticle interactions or/and surface disorder [46].

3. MATERIALS AND METHODS

CoCr2O4/SiO2 nanoparticles were synthesised by a sol–gel technique using cobalt nitrate (Co(NO3)2 6H2O), chromium nitrate (Cr(NO3)3 9H2O), citric acid (C6H8O7 H2O) and ammonia and tetraethyl orthosilicate (TEOS) materials with citric acid as a fuel agent. Sol–gel technique is defined as a low-cost, homogenous formation and non-destructive technique, which results from the uniform distribution of particle size. To obtain solution-1, 30 mL ethanol was used as a medium in which to stoichiometrically mix 99.9% pure (Co(NO3)2 6H2O) and (Cr(NO3)3 9H2O) salts. The distilled water and citric acid are mixed stoichiometrically in the desired ratio (0% and 80%) of TEOS to obtain solution-2. Solution-2 was injected drop-wise with a droplet in solution-1 to obtain solution-3. Some drops of ammonia were also introduced in solution-3 to maintain its pH value at 5. Solution-3 was stirred at 70°C to obtain its gel. The gel was dried in an oven at a temperature of 110°C for 12 h. The dry gel was ground for 2 h to obtain a homogeneous dry solution, and then the dry solution was purred in an alumina boat. The dry solution was annealed at 900°C for 4 h. The annealing results in the desired CoCr2O4/SiO2 nanoparticles. The single-phase crystalline structures of the CoCr2O4/(SiO2)y (y = 0 or 0.80) nanoparticles were confirmed with the use of XRD.

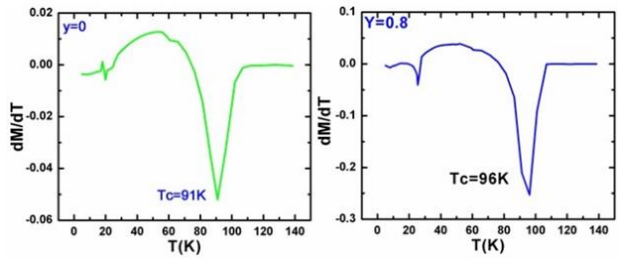

Fig. 10. Temperature dependence of magnetization and graph of dM/dT vs. T under magnetic field

4. CONCLUSIONS

T-dependent magnetic properties of CoCr2O4 nanoparticles without and with silica concentration were studied in detail. XRD patterns show the normal spinel structure of nanoparticles for the cases of both presence and absence of silica concentration. The average size of the crystal has reduced for nanoparticles with silica concentration due to the amorphous nature of silica, which confines the growth of nanoparticles. The ZFC/FC curves of cobalt chromite nanoparticles with and without silica concentration at 50 Oe, 500 Oe and 1,000 Oe have been studied. The values of *Tc* at 50 Oe, 500 Oe and 1,000 Oe were 99 K, 100 K and 101 K, respectively, for nanoparticles with no silica concentration. For SiO2-coated nanoparticles, *Tc* values at 50 Oe, 500 Oe and 1,000 Oe were 95 K, 99 K and 100 K, respectively. The values of *Ts* and *TL* were 27 K and 12 K, respectively, for nanoparticles with no silica concentration, which are found to be field-independent due

to strong lattice coupling as compared with nanoparticles with silica concentration. For cobalt chromite nanoparticles without silica concentration, the ZFC curve shows negative magnetisation, which perseveres up to 87 K due to the presence of uncompensated spin at grain boundaries, and this negative magnetisation has reduced for nanoparticles with silica concentration. The *Ms* value is decreased with decreasing temperature for nanoparticles without silica concentration. For nanoparticles with silica concentration, it reveals abnormal behaviour due to the amorphous nature of silica coating. At a temperature below 25 K, the *Ms* value is decreasing for nanoparticles without silica concentration, while it is increasing for nanoparticles with silica concentration. The *Hc* value is increased by reducing the temperature for both concentrations due to a reduction in thermal fluctuations at lower temperatures. The experimental data of *Hc* for both concentrations have been fitted by Kneller's law. The fitting parameters are $\alpha = 0.54$ and $TB = 75$ K for nanoparticles without silica concentration, and $\alpha = 1.59$ and $TB = 81$ K for those with silica concentration. In conclusion, SiO2 coating interferes with the disordered spin-spiral state ordering and decreases surface effects in these chromite nanoparticles.

REFERENCES

1. Hosseini SA, Alvarez-Galvan MC, Fierro JLG, Niaei A, Salari D. MCr2O4 (M= Co, Cu, and Zn) nanospinels for 2-propanol combustion: correlation of structural properties with catalytic performance and stability. Ceramics International. 2013;39(8):9253–61.
2. Knyazev AV, Mączka M, Bulanov EN, Ptak M, Belopolskaya SS. High-temperature thermal and X-ray diffraction studies, and room-temperature spectroscopic investigation of some inorganic pigments. Dyes and Pigments. 2011;91(3):286–93.
3. Avila AG, Barrera EC, Huerta LA, Muhl S. Cobalt oxide films for solar selective surfaces, obtained by spray pyrolisis. Solar Energy Materials and Solar Cells. 2004;82(1–2):269–78.
4. BaZr0.2Ce0.8−xYxO3−δ solid oxide fuel cell electrolyte synthesized by sol–gel combined with composition-exchange method - ScienceDirect [Internet]. [cited 2020 Jun 24]. Available from: https://www.sciencedirect.com/science/article/abs/pii/S036031991400384X
5. Effect of stoichiometry on (La0.6Sr0.4)xCo0.2Fe0.8O3 cathode evolution in solid oxide fuel cells - ScienceDirect [Internet]. [cited 2020 Jun 24]. Available from: https://www.sciencedirect.com/science/article/abs/pii/S0378775314008076
6. Fino D. Diesel emission control: Catalytic filters for particulate removal. Science and Technology of Advanced Materials [Internet]. 2007 Jan 1 [cited 2020 Jun 24];8(1–2):93–100. Available from: https://doi.org/10.1016/j.stam.2006.11.012
7. Eerenstein W, Mathur ND, Scott JF. Multiferroic and magnetoelectric materials. Nature [Internet]. 2006 Aug [cited 2020 Jun 24];442(7104):759–65. https://www.nature.com/articles/nature05023
8. Mancic L, Marinkovic Z, Vulic P, Moral C, Milosevic O. Morphology, Structure and Nonstoichiometry of ZnCr2O4 Nanophased Powder. Sensors [Internet]. 2003 Oct [cited 2020 Jun 24];3(10):415–23. Available from: https://www.mdpi.com/1424-8220/3/10/415
9. Anthony R. Solid state chemistry and its applications. John Wiley & Sons; 1990.
10. Choudhary P, Varshney D. Structural, vibrational and dielectric behavior of Co1-xMxCr2O4 (M = Zn, Mg, Cu and x = 0.0, 0.5) spinel chromites. Journal of Alloys and Compounds [Internet]. 2017 Nov 25 [cited 2020 Jun 24];725:415–24. Available from: http://www.sciencedirect.com/science/article/pii/S0925838817325380
11. Wang LG, Zhu CM, Chen L, Yuan SL. Exchange bias effect in CoCr2O4/NiO system prepared by two-step method. Solid State Communications [Internet]. 2017 Feb 1 [cited 2020 Jun 24];251:39–42. Available from: http://www.sciencedirect.com/science/article/pii/S0038109816303490
12. Gingasu D, Mindru I, Culita DC, Patron L, Calderon-Moreno JM, Osiceanu P, et al. Structural, magnetic and catalytic properties of cobalt chromite obtained through precursor method. Materials Research Bulletin [Internet]. 2015 Feb 1 [cited 2020 Jun 25];62:52–64. Available from: http://www.sciencedirect.com/science/article/pii/S0025540814006904
13. Lawes G, Melot B, Page K, Ederer C, Hayward MA, Proffen Th, et al. Dielectric anomalies and spiral magnetic order in ${\mathrm{CoCr}}_{2}{\mathrm{O}}_{4}$. Phys Rev B [Internet]. 2006 Jul 17 [cited 2020 Jun 24];74(2):024413. Available from:https://link.aps.org/doi/10.1103/PhysRevB.74.024413
14. Menyuk N, Dwight K, Wold A. Ferrimagnetic spiral configurations in cobalt chromite. J Phys France [Internet]. 1964 May 1 [cited 2020 Jun 24];25(5):528–36. Available from: http://dx.doi.org/10.1051/jphys:01964002505052801
15. Manikandan A, Sridhar R, Arul Antony S, Ramakrishna S. A simple aloe vera plant-extracted microwave and conventional combustion synthesis: Morphological, optical, magnetic and catalytic properties of CoFe2O4 nanostructures. Journal of Molecular Structure [Internet]. 2014 Nov 5 [cited 2020 Jun];1076:188–200.http://www.sciencedirect.com/science/article/pii/S002228601400790X
16. Rath C, Mohanty P. Magnetic Phase Transitions in Cobalt Chromite Nanoparticles. J Supercond Nov Magn [Internet]. 2011 Jan 1 [cited 2020 Jun 24];24(1):629–33. Available from: https://doi.org/10.1007/s10948-010-0958-7
17. Galivarapu JK, Kumar D, Banerjee A, Sathe V, Aquilanti G, Rath C. Effect of size reduction on cation distribution and magnetic transitions in CoCr2O4 multiferroic: EXAFS, magnetic and diffused neutron scattering measurements. RSC Adv [Internet]. 2016 Jul 1 [cited 2020 Jun 24];6(68):63809–19. Available from : https://pubs.rsc.org/en/content/articlelanding/2016/ra/c6ra10189e
18. Huang DJ, Okamoto J, Huang SW, Mou CY. Magnetic Transitions of Multiferroic Frustrated Magnets Revealed by Resonant Soft X-ray Magnetic Scattering. J Phys Soc Jpn [Internet]. 2010 Jan 12 [cited 2020 Jun 24];79(1):011009. Available from: https://journals.jps.jp/doi/abs/10.1143/JPSJ.79.011009
19. Chen CC, Herhold AB, Johnson CS, Alivisatos AP. Size Dependence of Structural Metastability in Semiconductor Nanocrystals. Science [Internet]. 1997 Apr 18 [cited 2020 Jun 24];276(5311):398–401. Available from: https://science.sciencemag.org/content/276/5311/398
20. Tsoukatos A, Wan H, Hadjipanayis GC, Papaefthymiou V, Kostikas A, Simopoulos A. Origin of coercivity in (Fe,Co)-based granular films. Journal of Applied Physics [Internet]. 1993 May 15 [cited 2020 Jun 24];73(10):6967–9. Available from:https://aip.scitation.org/doi/abs/10.1063/1.352399
21. Hee Kim E, Sook Lee H, Kook Kwak B, Kim BK. Synthesis of ferrofluid with magnetic nanoparticles by sonochemical method for MRI contrast agent. Journal of Magnetism and Magnetic Materials [Internet]. 2005 Mar 1 [cited 2020 Jun 24];289:328–30. Available from: http://www.sciencedirect.com/science/article/pii/S0304885304013186
22. Nadeem K, Ali L, Gul I, Rizwan S, Mumtaz M. Effect of silica coating on the structural, dielectric, and magnetic properties of maghemite nanoparticles. Journal of Non-Crystalline Solids [Internet]. 2014 Nov 15 [cited 2020 Jun 24];404:72–7. Available from: http://www.sciencedirect.com/science/article/pii/S0022309314003494
23. Abarra EN, Gill P, Min Zheng, Zhou JN, Acharya BR, Choe G. Preconditioning, write width, and recording properties of Co-Cr-Pt-O perpendicular media with various underlayer designs. IEEE Transactions on Magnetics. 2005 Feb;41(2):581–6.
24. Wu KH, Chang YC, Wang GP. Preparation of NiZn ferrite/SiO2 nanocomposite powders by sol–gel auto-combustion method. Journal of Magnetism and Magnetic Materials [Internet]. 2004 Feb 1 [cited 2020 Jun 24];269(2):150–5. Available from:http://www.sciencedirect.com/science/article/pii/S0304885303005857

25. Chaudhuri A, Mandal M, Mandal K. Preparation and study of NiFe2O4/SiO2 core–shell nanocomposites. Journal of Alloys and Compounds [Internet]. 2009 Nov 13 [cited 2020 Jun 24];487(1):698–702. Available from: http://www.sciencedirect.com/science/article/pii/S0925838809016089
26. Zhang S, Dong D, Sui Y, Liu Z, Wang H, Qian Z, et al. Preparation of core shell particles consisting of cobalt ferrite and silica by sol–gel process. Journal of Alloys and Compounds [Internet]. 2006 May 18 [cited 2020 Jun 24];415(1):257–60. Available from: http://www.sciencedirect.com/science/article/pii/S0925838805012661
27. Kamran M, Ullah A, Mehmood Y, Nadeem K, Krenn H. Role of SiO2 coating in multiferroic CoCr2O4 nanoparticles. AIP Advances [Internet]. 2017 Feb 1 [cited 2020 Jun 24];7(2):025011. Available from: https://aip.scitation.org/doi/full/10.1063/1.4973732
28. Nadeem K, Krenn H, Shahid M, Letofsky-Papst I. Influence of SiO2 matrix and annealing time on properties of Ni-ferrite nanoparticles. Solid State Sciences [Internet]. 2013 May 1 [cited 2020 Jun 24];19:27–31. Available from: http://www.sciencedirect.com/science/article/pii/S129325581300068X
29. Zi Z, Sun Y, Zhu X, Yang Z, Dai J, Song W. Synthesis and magnetic properties of CoFe2O4 ferrite nanoparticles. Journal of Magnetism and Magnetic Materials [Internet]. 2009 May 1 [cited 2020 Jun 24];321(9):1251–5. Available from: http://www.sciencedirect.com/science/article/pii/S0304885308011578
30. Gopalan EV, Joy PA, Al-Omari IA, Kumar DS, Yoshida Y, Anantharaman MR. On the structural, magnetic and electrical properties of sol–gel derived nanosized cobalt ferrite. Journal of Alloys and Compounds [Internet]. 2009 Oct 19 [cited 2020 Jun 24];485(1):711–7. Available from: http://www.sciencedirect.com/science/article/pii/S0925838809012092
31. Krenke T, Acet M, Wassermann EF, Moya X, Mañosa L, Planes A. Ferromagnetism in the austenitic and martensitic states of $\mathrm{Ni}\text{\ensuremath{-}}\mathrm{Mn}\text{\ensuremath{-}}\mathrm{In}$ alloys. Phys Rev B [Internet]. 2006 May 15 [cited 2020 Jun 24];73(17):174413. Available from: https://link.aps.org/doi/10.1103/PhysRevB.73.174413
32. Kahn O. The magnetic turnabout. Nature [Internet]. 1999 May [cited 2020 Jun 24];399(6731):21–2. Available from: https://www.nature.com/articles/19862
33. Ohkoshi S ichi, Yorozu S, Sato O, Iyoda T, Fujishima A, Hashimoto K. Photoinduced magnetic pole inversion in a ferro–ferrimagnet: (Fe0.40IIMn0.60II)1.5CrIII(CN)6. Appl Phys Lett [Internet]. 1997 Feb 24 [cited 2020 Jun 24];70(8):1040–2. Available from: https://aip.scitation.org/doi/abs/10.1063/1.118475
34. Plocek J, Holec P, Kubickova S, Pacakova B, Matulkova I, Mantlikova A, et al. Stabilization of Transition Metal Chromite Nanoparticles in Silica Matrix. International Journal of Chemical and Molecular Engineering [Internet]. 2014 Oct 5 [cited 2020 Jun 24];8(11):1219–28. Available from: http://publications.waset.org/9999702/stabilization-of-transition-metal-chromite-nanoparticles-in-silica-matrix
35. Plumier R. Reinvestigation of Magnetic Structures of CoCr2O4 and MnCr2O4 Obtained by Neutron Diffraction. Journal of Applied Physics [Internet]. 1968 Feb 1 [cited 2020 Jun 24];39(2):635–6. Available from: https://aip.scitation.org/doi/abs/10.1063/1.2163559
36. Mufti N, Nugroho AA, Blake GR, Palstra TTM. Magnetodielectric coupling in frustrated spin systems: the spinels MCr2O4(M = Mn, Co and Ni). J Phys: Condens Matter [Internet]. 2010 Feb [cited 2020 Jun 24];22(7):075902. Available from: https://doi.org/10.1088%2F0953-8984%2F22%2F7%2F075902
37. Tang ZX, Chen JP, Sorensen CM, Klabunde KJ, Hadjipanayis GC. Tang et al. reply. Phys Rev Lett [Internet]. 1992 May 18 [cited 2020 Jun 24];68(20):3114–3114. Available from: https://link.aps.org/doi/10.1103/PhysRevLett.68.3114
38. Binder K. Statistical mechanics of finite three-dimensional Ising models. Physica [Internet]. 1972 Dec 15 [cited 2020 Jun 24];62(4):508–26. Available from: http://www.sciencedirect.com/science/article/pii/0031891472902376
39. Tartaj P, González-Carreño T, Serna CJ. Magnetic Behavior of γ-Fe2O3 Nanocrystals Dispersed in Colloidal Silica Particles. J Phys Chem B [Internet]. 2003 Jan 1 [cited 2020 Jun 24];107(1):20–4. Available from: https://doi.org/10.1021/jp0260898
40. Grinbom G, Duveau D, Gershinsky G, Monconduit L, Zitoun D. Silicon/Hollow γ-Fe2O3 Nanoparticles as Efficient Anodes for Li-Ion Batteries. Chem Mater [Internet]. 2015 Apr 14 [cited 2020 Jun 24];27(7):2703–10. Available from: https://doi.org/10.1021/acs.chemmater.5b00730
41. Zeb F, Nadeem K, Shah SKA, Kamran M, Gul IH, Ali L. Surface spins disorder in uncoated and SiO2 coated maghemite nanoparticles. Journal of Magnetism and Magnetic Materials [Internet]. 2017 May 1 [cited 2020 Jun 24];429:270–5. Available from: http://www.sciencedirect.com/science/article/pii/S0304885316313762
42. Caizer C, Stefanescu M. Magnetic characterization of nanocrystalline Ni Zn ferrite powder prepared by the glyoxylate precursor method. J Phys D: Appl Phys [Internet]. 2002 Nov [cited 2020 Jun 24];35(23):3035–40. Available from: https://doi.org/10.1088%2F0022-3727%2F35%2F23%2F301
43. Aslibeiki B, Kameli P. Magnetic properties of MnFe2O4 nanoaggregates dispersed in paraffin wax. Journal of Magnetism and Magnetic Materials [Internet]. 2015 Jul 1 [cited 2020 Jun 25];385:308–12. Available from: http://www.sciencedirect.com/science/article/pii/S0304885315002449
44. Xu ST, Ma YQ, Zheng GH, Dai ZX. Simultaneous effects of surface spins: rarely large coercivity, high remanence magnetization and jumps in the hysteresis loops observed in CoFe2O4 nanoparticles. Nanoscale [Internet]. 2015 Apr 2 [cited 2020 Jun 25];7(15):6520–6. Available from: https://pubs.rsc.org/en/content/articlelanding/2015/nr/c5nr00582e
45. Obaidat IM, Issa B, Albiss BA, Haik Y. Temperature Dependence of Saturation Magnetization and Coercivity in Mn0.5Zn0.5Gd0.02Fe1.98O4Ferrite Nanoparticles. IOP Conf Ser: Mater Sci Eng [Internet]. 2015 Oct [cited 2020 Jun 25];92:012012. Available from: https://doi.org/10.1088%2F1757-899x%2F92%2F1%2F012012
46. Kneller EF, Luborsky FE. Particle Size Dependence of Coercivity and Remanence of Single-Domain Particles. Journal of Applied Physics [Internet]. 1963 Mar 1 [cited 2020 Jun 25];34(3):656–8. Available from: https://aip.scitation.org/doi/abs/10.1063/1.1729324

Acknowledgments: The authors are grateful to the Researchers Supporting Project (No. RSPD2023R667), King Saud University, Riyadh, Saudi Arabia. The authors also acknowledge the Department of Physics at the International Islamic University and ORIC MUST (Nos 1124/2019 and 172/2020).

Ghazanfar Mehboob: https://orcid.org/0009-0009-3912-1743
Amjad Iqbal: https://orcid.org/0000-0001-7405-0324
Mohamed Ragab: https://orcid.org/0000-0001-8878-760X
Sohaib Ajmal: https://orcid.org/0000-0002-3234-943X
Adel El-Marghany: https://orcid.org/0009-0002-6464-7113